Supplementary Materials for

Driving a Macroscopic Oscillator with the Stochastic Motion of a Hydrogen Molecule

Christian Lotze, Martina Corso, Katharina J. Franke,
Felix von Oppen, Jose Ignacio Pascual*

*To whom correspondence should be addressed. E-mail: ji.pascual@nanogune.eu

Published 9 November 2012, *Science* **338**, 779 (2012)
DOI: 10.1126/science.1227621

This PDF file includes:

Supporting online material to the manuscript: Driving a macroscopic oscillator by the stochastic motion of a hydrogen molecule

Christian Lotze,[1] Martina Corso,[1] Katharina J. Franke,[1] Felix von Oppen,[1,2] and Jose Ignacio Pascual[1]

[1] *Fachbereich Physik, Freie Universität Berlin, 14195 Berlin, Germany*
[2] *Dahlem Center for Complex Quantum Systems, Freie Universität Berlin, 14195 Berlin, Germany*

1 Materials and methods

1.1 Experimental details

Our measurements have been realized in ultra high vacuum (UHV), using a low temperature (base temperature 5 K) scanning tunneling microscope equipped with a qPlus sensor [2] and provided by Createc GmbH [1]. A digital Phase-lock Loop (PLL) algorithm is used (Createc GmbH and by Nanonis GmbH [3]) to track the resonance frequency of the oscillator at constant amplitude of tip oscillation A_{osc}.

We use a single crystal Cu(111) sample as substrate. The surface is cleaned by repetitive cycles of Ne^+ ion sputtering and annealing, until the resulting surface is atomically clean and flat. Hydrogen molecules are deposited on the cold sample, directly placed at the LT-STM stage. We backfilled the UHV chamber with a H_2 pressure in the order of $5\times\ 10^7$ mbar and open the access to the STM for a few minutes. By controlling the dosing pressure and time, the H_2 coverage can be controlled. At the lowest coverages H_2 molecules are hardly visible in the STM images. After extended H_2 doses, the appearance of a H_2 layer with a characteristic hexagonal structure is observed.

The fingerprint of electron-induced H_2 fluctuations and its effect driving the tip self-oscilaltion, is observed independently of the coverage, at bias values around V_{th}. A larger H_2 coverages the threshold bias V_{th} increases, as shown in reference [5].

To avoid a cross-talk between tunneling current and qPlus sensor, which could eventually cause self-oscillations, the STM tip is electrically decoupled from the holding prong by non-conductive epoxy, and the tunneling current extracted via a 12.5μm gold wire connected to it [6]. The results presented here are acquired with a preamplifier gain of 10^5 and bandwidth well above the oscillator's resonance frequency, and reproduced with various gains. In this way, we avoid the saturation of the preamplifier at frequencies larger than our bandwidth, which could eventually induce a capacitive coupling of the force sensor and tip potential. We can also exclude slew-rate dependent potential changes between the inverting and non-inverting input of the current preamplifier due to the nonlinear current fluctuations. The absence of a bias effect in the frequency shift is routinely probed for the conditions of the experiments shown here.

1.2 Measurement of energy dissipation

The motion of an oscillator with $X(t)=A_{osc}\cdot\cos(\omega_0 t)$ has stored energy $E = \frac{k}{2}A_{osc}^2$, where k is its force constant. The energy dissipated during the motion is determined by its quality factor Q [7], so that an energy $D_0 = \frac{2\pi E}{Q} = \frac{\pi k}{Q}A_{osc}^2$ per cycle is required to maintain the oscillation at constant amplitude A_{osc}. This energy per cycle (i.e. power) is provided by an external driving signal $A_{Drive}(t) = A_D \cdot \cos(\omega_0 t + \phi)$ applied to a piezoelectric actuator holding the qPlus sensor, with a phase shift $\phi = \pi/2$ with respect to the tip oscillation. We calibrate A_D for each qPlus sensor oscillating with amplitude A_{osc} far away from the sample. This allows us to associate A_D to a value of energy dissipated per cycle.

Close to the surface, the tip oscillates around a position X_0 set by the STM feedback parameters (I_t, V_s). Here, there are additional interactions which may modify the dynamics of the oscillator and, therefore, the driving signal for keeping A_{osc} constant. The energy dissipation per cycle is then estimated from the relation $D = D_0\frac{A_D}{A_D^f}$, where the superscript f relates to the driving amplitude of the free tip [2]. The magnitude D is plotted in Fig. 2E & 2F of the manuscript, in units of D_0=7 meV/cycle.

The electronic system used in the data of Fig. 2 [3]

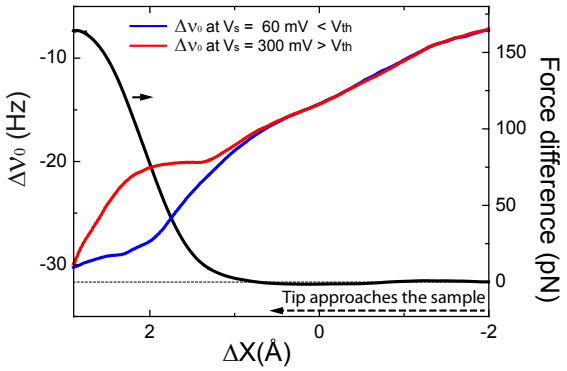

FIG. 1: Plot of frequency shift vs. tip approach distance measured at sample bias well above and below the threshold bias V_{th}(A_{osc}=70 pm, ν_0=20.730 kHz). The approach distance is with respect a tip position set with I_t=0.5 nA and V_s= 300 mV. The two plots show a marked difference when the tip approaches to short distances from the sample. We interpret these differences as two different force fields with distinct force gradients. The black curve plots the integrated difference of the $\Delta\nu_0$ curves, converted to forces as explained in the text.

reacts with negative A_D values to the self oscillation. This corresponds to a shift of $-\pi/2$ between the driving and oscillation signals, i.e. a phase reversal, which counteracts the growing amplitudes caused by the self-oscillation.

2 Supporting results

2.1 Estimation of the amplitude of force fluctuations

The frequency shift of a qPlus sensor $\Delta\nu_0$ is proportional to k_{ts}, the stiffness of the tip and sample junction, when it oscillates with sub-Ångstrom amplitudes and if only conservative forces apply [2]. In this case, $k_{ts} = 2k\frac{\Delta\nu_0}{\nu_0}$, with k being the stiffness of the free sensor (1800 N/m), and the corresponding force field can be estimated by integrating k_{ts} along a specific coordinate [8]. The assumption of conservative forces does not apply close to the threshold bias V_{th}, where the molecule fluctuates. However, far from this bias value it is a reasonable assumption in view of the measured dissipation value, which is close to that of the free sensor D_0. Here, we provide an estimate of the force fluctuation by accounting for the force difference between the two regimes, estimated far from V_{th}.

Fig. 1 compares two plots of $\Delta\nu_0$ as a function of tip displacement ΔX. Before starting the tip approach at ΔX=-2Å, the bias is adjusted to 60 mV (blue) and 300 mV (red), values far from the bias threshold $V_{th}\sim$ 150 mV. Both $\Delta\nu_0$-ΔX plots coincide at larger tip-sample separations in a smooth negative $\Delta\nu_0$ background. This

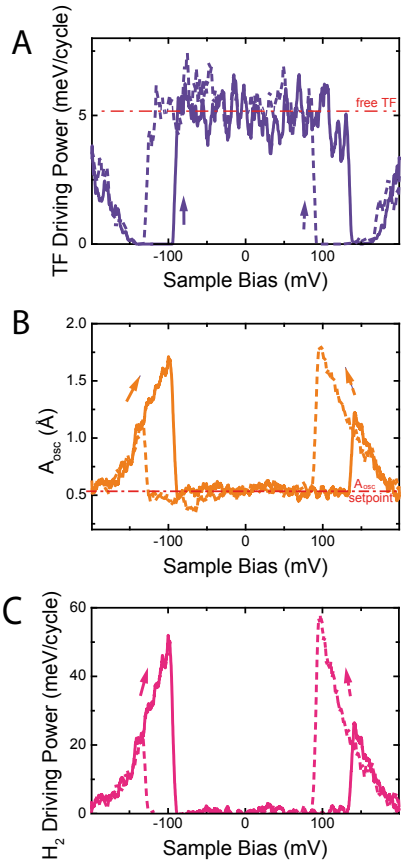

FIG. 2: Bias dependence of (A) the driving power (obtained from A_D, using the method described in the text) and (B) the amplitude of tip oscillation for a H_2 junction. During the acquisition only positive values of the driving amplitude were allowed. This results in a increase of A_{osc} beyond the setpoint value of 50 pm when the self-oscillation appears, around V_{th}. (ν_0=23.920 kHz). (C) Plot of the corresponding power generated by the H_2 molecule to drive the tuning fork self oscillation (details in text). The spectra shows a pronounced hysteresis because the increase in oscillation amplitude also affects the onset for TLFs.

background is due to long-range attractive forces (van der Waals and electrostatic) between the mesoscopic tip apex and the surface. At close distances, however, the plots deviate from the smooth background in a different manner. For V_s<V_{th}(regime 1) the frequency shift increases more steeply. We attribute this to the presence of short-range attractive forces. For V_s>V_{th}, the frequency shift tends to decrease, denoting a slight compensation of the background attractive forces. We estimate the force difference between the two states Δf=f_2−f_1 by deconvoluting both $\Delta\nu_0$ signals using the method by Sader and Jarvis [9] and integrating their difference along the tip-sample distance X. Δf grows as the tip approaches, reaching more than 150 pN at the closest position inspected.

2.2 Estimation of driving power of a H_2 junction

Fig. 2 shows spectra of a H_2 junction obtained by allowing only positive values of the driving signal ($A_D \geq 0$). The self oscillation of the tuning fork at $\pm V_{th}$ causes the suppression of A_D near this bias (shown in Fig. 2A converted to applied power $D = D_0 \frac{A_D}{A_D^f}$) and the increase of the oscillation amplitude beyond the 50 pm setpoint. The tip reaches oscillation amplitudes of more than 1.5 Å driven solely by the H_2 molecule. The driving power produced by the fluctuations of the H_2 molecule can be estimated using the expression from above to be $D_{H_2} = \frac{\pi k}{Q} A_{osc}^2 - D$[2], which is plotted in Fig. 2C. The H_2 molecule produces more than 50 meV per cycle, a factor of ten larger than the intrinsic dissipation of the tuning fork.

Theoretical modeling

In this section, we provide more details of the theoretical modeling and estimates, justifying and extending the considerations in the main body of the manuscript.

3.1 Force due to tip-substrate interaction

We begin by considering the tip-substrate interaction. The experimental observations imply that the tip oscillator is subject to different tip-substrate forces, denoted by f_1 and f_2 with $\Delta f = f_2 - f_1$, for the two switching states of the hydrogen molecule. Thus, the current-induced switching of the hydrogen molecule yields a stochastic force $f(t)$ acting on the oscillator and, in a simple linear model, the oscillator displacement $X(t)$ obeys the equation of motion

$$\ddot{X} + 2\gamma\dot{X} + \omega_0^2 X = \frac{f(t)}{M}, \tag{1}$$

where M denotes the effective mass of the oscillator and ω_0 its eigenfrequency. The damping coefficient γ is related to the (bare) quality factor Q of the mechanical oscillator through $Q = \omega_0/2\gamma$. Here, we have assumed that the oscillator obeys a linear equation. We will consider the implications of nonlinear corrections further below.

To understand the switching-induced motion of the oscillator, we need to investigate the stochastic force $f(t)$. To do so, we define variables $n_i(t)$ which take on the value 1 when the hydrogen molecule is in state $i = 1, 2$, and 0 otherwise [so that $n_1(t) + n_2(t) = 1$ at all times t]. The force $f(t)$ can then be expressed as

$$f(t) = f_1 n_1(t) + f_2 n_2(t). \tag{2}$$

The statistics of the occupations $n_i(t)$ (and thus of $f(t)$) can be obtained from the Markovian Master equation

$$\frac{dn_1(t)}{dt} = -\Gamma_1(t) n_1 + \Gamma_2(t)[1 - n_1(t)], \tag{3}$$

where $\Gamma_i(t)$ denotes the inverse dwell times of the hydrogen molecules in states $i = 1, 2$. The assumption of a Markovian Master equation is justified since the rate of electron tunneling is fast compared to all time scales of the oscillator and only a small fraction of tunneling electrons switch the state of the hydrogen molecule.

In general, we allow for an arbitrary time dependence of the rates $\Gamma_i(t)$. We first consider these rates as independent of the oscillator displacement and thus time independent. With this approximation, the solution of the Master equation with initial condition $n_i(t_0)$ becomes

$$n_i(t) = \frac{\Gamma_{\bar{i}}}{\Gamma} + \left[n_i(t_0) - \frac{\Gamma_{\bar{i}}}{\Gamma} \right] e^{-\Gamma(t - t_0)}, \tag{4}$$

where we introduced the notation $\bar{1} = 2$ and $\bar{2} = 1$ as well as $\Gamma = \Gamma_1 + \Gamma_2$. In the limit $t_0 \to -\infty$, this reduces to the stationary solution

$$\langle n_i \rangle = n_i(t \to \infty) = \frac{\Gamma_{\bar{i}}}{\Gamma}, \tag{5}$$

yielding the average of the force $f(t)$,

$$\langle f \rangle = \frac{f_1 \Gamma_2 + f_2 \Gamma_1}{\Gamma_1 + \Gamma_2}. \tag{6}$$

The equation of motion (1) implies that this average force merely shifts the equilibrium position of the oscillator displacement $X(t)$ so that it can be absorbed by an (implicit) shift of $X(t)$.

The motion of the oscillator is driven by the fluctuations about the average, $\delta f(t) = f(t) - \overline{f}$. Its correlation function can be readily obtained from the general solution (4) of the Master equation (3),

$$\langle \delta f(t)\, \delta f(t') \rangle = (\Delta f)^2 \frac{\Gamma_1 \Gamma_2}{\Gamma^2} e^{-\Gamma |t - t'|}. \tag{7}$$

Fourier transforming yields the spectral density

$$\langle |\delta f_\omega|^2 \rangle = (\Delta f)^2 \frac{2\Gamma_1 \Gamma_2 / \Gamma}{\omega^2 + \Gamma^2}. \tag{8}$$

of the fluctuating force. Note that the characteristic frequency of the spectral density is given by the total switching rate Γ and that for fixed Γ, the overall prefactor becomes maximal when the rates Γ_1 and Γ_2 are of the same order.

3.2 Driven oscillations

The force fluctuations $\delta f(t)$ drive the oscillator and we can now estimate the amplitude of the resulting driven

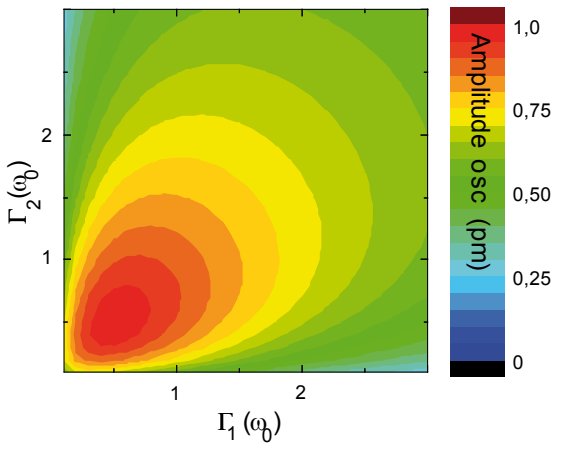

FIG. 3: Plot of the amplitude of oscillation as a function of the rates of molecular motion out of state 1 and 2, Γ_1 and Γ_2, respectively, following equation (11). The maximum oscillation occurs for $\Gamma_{1,2} = \omega_0/2$.

motion of the oscillator. From the equation of motion (1), we find

$$X_\omega = \frac{1/M}{\omega_0^2 - \omega^2 - 2i\gamma\omega}\,\delta f_\omega \tag{9}$$

for the Fourier components of the oscillator displacement, so that

$$\begin{aligned}\langle |X_\omega|^2\rangle &= \frac{1/M^2}{(\omega_0^2-\omega^2)^2+4\gamma^2\omega^2}\,\langle|\delta f_\omega|^2\rangle \\ &\simeq \frac{1/4M^2\omega_0^2}{(\omega-\omega_0)^2+\gamma^2}\,\langle|\delta f_\omega|^2\rangle. \end{aligned}\tag{10}$$

Here, the second line is valid in the limit of a weakly damped oscillator, $Q \gg 1$. Inserting Eq. (8) and Fourier transforming back to time yields

$$\langle (X(t))^2\rangle \simeq \frac{\Delta f^2}{8\omega_0^2\gamma M^2}\,\frac{2\Gamma_2\Gamma_1/(\Gamma_2+\Gamma_1)}{\omega_0^2+(\Gamma_2+\Gamma_1)^2}. \tag{11}$$

The stochastic nature of the driving force is reflected in the scaling of the oscillation amplitude with the quality factor, $X(t) \sim Q^{1/2}$.

The optimal amplitude follows for $\Gamma_1 = \Gamma_2 = \Gamma/2$ and $\Gamma = \omega_0$ (figure 3) and yields

$$\langle (X(t))^2\rangle_{\rm opt} \simeq \frac{\Delta f^2}{32\omega_0^3\gamma M^2}. \tag{12}$$

We can estimate this maximal amplitude of the driven motion of the oscillator for the parameters of the experiment. Using the standard parameters of our qPlus sensor $\omega_0 \simeq 10^5 {\rm s}^{-1}$, $M \simeq 0.1$ mg (or, equivalently, spring constant $k \sim$1800 N/m), and Q$\sim 10^4$ (or $\gamma \sim 10{\rm s}^{-1}$), as well as the observed force difference $\Delta f \sim 100$ pN, Eq. (12) yields an upper limit to the driven oscillations of the tip of order ~ 0.1 Å. This estimate shows that the observed self-oscillations of the cantilever cannot be explained as driven oscillations of the qPlus sensor.

3.3 Stochastic resonance and self-oscillations

In order to explain the observed self-oscillations, we go beyond the assumption of switching rates which are independent of the cantilever displacement. This provides a feedback mechanism by making the average force $\langle f(t)\rangle$ dependent on the cantilever displacement. To linear order in the cantilever displacement, the tip-substrate interaction causes a renormalization of both the restoring force and, importantly, the friction force acting on the cantilever. Self-oscillations of the cantilever occur when the renormalized friction coefficient becomes *negative*.

Microscopically, the switching rates are functions of the cantilever displacement for several reasons:

- The tunneling current is a sensitive function of the cantilever displacement. Assuming that each tunneling electron has a small, but finite chance to switch the hydrogen molecule, this makes the switching rates dependent on cantilever displacement. We will see below that this modifies the occupation probabilities of the two molecular states only weakly since it affects both rates, Γ_1 and Γ_2, in the same manner.

- As the cantilever displacement changes at fixed bias voltage, the electric field in the junction changes, causing a modification of the double-well potential of the cantilever and, with it, the transfer rates Γ_1 and Γ_2 between them. We note that this effect has previously been demonstrated experimentally by Gupta *at al.* [5]. As one can see from Fig. 2, increasing the tip-substrate distance causes an increase in the threshold bias, making the low-bias state of the molecule more favorable. We find that this dependence of the switching rates on cantilever displacement has a larger effect on the oscillations of the resonator because the effects on Γ_1 and Γ_2 are anticorrelated.

To incorporate the dependence of the switching rates on cantilever displacement into our modeling, we solve the Master equation (3) for arbitrary time-dependent rates $\Gamma_1(t)$ and $\Gamma_2(t)$. With arbitrary initial conditions $n_i(t_0)$, one obtains

$$n_1(t) = g(t)\left[n_1(t_0) + \int_{t_0}^{t} d\tau \Gamma_2(\tau) g^{-1}(\tau)\right], \tag{13}$$

where

$$g(t) = \exp\{-\int_{t_0}^{t} d\tau[\Gamma_1(\tau)+\Gamma_2(\tau)]\}. \tag{14}$$

as well as the solution for $n_2(t) = 1 - n_1(t)$.

This solution allows us to proceed analytically, if we approximate the changes in $\Gamma_i(t)$ to linear order in the oscillator displacements $X(t)$,

$$\Gamma_i(t) \simeq \Gamma_i + \Gamma_i' X(t). \tag{15}$$

Here, $\Gamma_i' = d\Gamma_i/dX$. In view of the oscillations of the tip, this yields a Master equation (3) with oscillatory switching rates, a problem known in the literature as stochastic resonance [10]

Starting with the general solution (13) and inserting (15), we can compute the occupations $n_i(t)$ to linear order in the oscillator displacement and obtain

$$\begin{aligned} n_1(t) &= \frac{\Gamma_2}{\Gamma} + \frac{\Gamma_1}{\Gamma} e^{-\Gamma(t-t_0)} \\ &+ \frac{\Gamma_2'\Gamma_1 - \Gamma_1'\Gamma_2}{\Gamma} \int_{t_0}^{t} d\tau X(\tau) e^{-\Gamma(t-\tau)} \\ &- \frac{\Gamma_1(\Gamma_1' + \Gamma_2')}{\Gamma} e^{-\Gamma(t-t_0)} \int_{t_0}^{t} d\tau X(\tau) \end{aligned} \tag{16}$$

for the initial condition $n_1(t_0) = 1$. Taking the limit $t_0 \to -\infty$, we obtain the stationary result

$$n_1(t) = \frac{\Gamma_2}{\Gamma} + \frac{\Gamma_2'\Gamma_1 - \Gamma_1'\Gamma_2}{\Gamma} \int_{-\infty}^{t} d\tau X(\tau) e^{-\Gamma(t-\tau)} \tag{17}$$

and, consequently,

$$n_2(t) = \frac{\Gamma_1}{\Gamma} - \frac{\Gamma_2'\Gamma_1 - \Gamma_1'\Gamma_2}{\Gamma} \int_{-\infty}^{t} d\tau X(\tau) e^{-\Gamma(t-\tau)}. \tag{18}$$

The first terms on the right-hand sides of Eqs. (17) and (18) reproduce the result obtained above for time-independent switching rates, while the second terms originate from the dependence of the switching rates on cantilever displacement. It is these second terms which are refered to as stochastic resonance as they are particularly pronounced when the frequency of the oscillator is of the order of the total stochastic switching rate Γ. Clearly, the stochastic resonance terms are larger when Γ_1' and Γ_2' have opposite signs. For this reason, we will focus on the dependence of Γ_i with cantilever displacement due to modifications of the double-well potential.

We can now insert Eqs. (17) and (18) into Eq. (2) for the time-dependent force acting on the cantilever,

$$\begin{aligned} f(t) &= \frac{\Gamma_2 f_1 + \Gamma_1 f_2}{\Gamma} \\ &+ (\Delta f) \frac{\Gamma_2'\Gamma_1 - \Gamma_1'\Gamma_2}{\Gamma} \int_{-\infty}^{t} d\tau X(\tau) e^{-\Gamma(t-\tau)}. \end{aligned} \tag{19}$$

The essential consequences for the motion of the oscillator are brought out most clearly by Fourier transforming $f(t)$ to the frequency domain, yielding

$$\begin{aligned} f_\omega &= 2\pi\delta(\omega) \frac{\Gamma_2 f_1 + \Gamma_1 f_2}{\Gamma} \\ &+ (\Delta f) \frac{\Gamma_2'\Gamma_1 - \Gamma_1'\Gamma_2}{\Gamma} \frac{1}{-i\omega + \Gamma} X_\omega. \end{aligned} \tag{20}$$

The reactive part, $\mathrm{Re} f_\omega$, of the force $f(t)$ causes a weak modification of the restoring force acting on the cantilever and, consequently, of the resonance frequency $\omega = \omega_0 + \Delta\omega$. The "dissipative" component, $\mathrm{Im} f_\omega$, of $f(t)$,

$$\mathrm{Im} f_\omega = (\Delta f) \frac{\Gamma_2'\Gamma_1 - \Gamma_1'\Gamma_2}{\Gamma} \frac{\omega}{\omega^2 + \Gamma^2} X_\omega \tag{21}$$

can have more dramatic consequences. The reason is that this switching-induced contribution to the "friction" force does not have a fixed sign and can thus correspond to a *negative* damping coefficient. The requirement of positive damping follows from the stability of the thermodynamic equilibrium state, a condition that no longer applies in the present non-equilibrium situation of current-induced switching.

A comparison with the Fourier transform $i\omega 2\gamma X_\omega$ of the regular friction force $-2\gamma\dot{X}$ shows that the "dissipative" feedback force $\mathrm{Im} f_\omega$ causes a renormalization of the damping coefficient, so that the cantilever becomes subject to the effective damping coefficient

$$\gamma_{\mathrm{eff}}(\omega) = \gamma + \frac{(\Delta f)}{M} \frac{\Gamma_2'\Gamma_1 - \Gamma_1'\Gamma_2}{2\Gamma} \frac{1}{\omega^2 + \Gamma^2}. \tag{22}$$

Indeed, the switching-induced contribution to the damping is negative in our setup. We define X such that it increases with increasing tip-substrate distance. Since the cantilever is attracted to the substrate, we have $f_1, f_2 < 0$. Experimentally, we find that the force is larger in magnitude for the low-voltage state, say state 1, such that $\Delta f = f_1 - f_2 < 0$. Since the low-voltage state becomes more stable at larger X (see discussion above), we conclude that $\Gamma_2' > 0$ as well as $\Gamma_1' < 0$.

The equilibrium position of the cantilever in the absence of current-induced switching becomes unstable when the current-induced "dissipative" force (21) overcompensates the intrinsic damping coefficient γ, making the overall renormalized damping γ_{eff} negative. In line with experimental observations, this is most likely to occur when the cantilever frequency ω_0 is of the order of the total switching rate Γ, so that

$$\Delta\gamma_{\mathrm{eff}}(\omega) \sim -|\Delta f| \frac{|\Gamma_1'|}{\mathrm{M}\omega_0^2}. \tag{23}$$

In fact, we can estimate the switching-induced renormalization of the damping coefficient, using $\Gamma \sim \omega_0 \simeq 10^5 \mathrm{s}^{-1}$, $\Gamma_i' \sim \Gamma/1\mathrm{nm}$, making the (conservative) assumption that the switching rates change over the characteristic length of 1nm in cantilever displacement, and $\Delta f \sim 100\mathrm{pN}$, as measured experimentally. This yields a switching induced correction of order $\Delta\gamma_{\mathrm{eff}} \sim -10\mathrm{s}^{-1}$. This should be compared with the bare friction coefficient $\gamma \sim M\omega_0/Q \sim 10\mathrm{s}^{-1}$. This shows that the effective damping γ_{eff} can indeed be negative.

3.4 Self-oscillation amplitude

To linear order in the displacement $X(t)$, a negative damping coefficient causes an exponential instability and the oscillation amplitude grows without bound. In real cantilevers, the instability will be limited by nonlinear effects. To study the resulting oscillation amplitude within a minimal model, we include a weak cubic (Duffing) nonlinearity in the equation of motion for an oscillator with *negative* damping coefficient δ,

$$\ddot{X} - 2\delta\dot{X} + \omega_0^2 X + \alpha X^3 = 0. \tag{24}$$

This model incorporates the switching-induced force on the cantilever through an effective negative damping coefficient δ (taken to be frequency independent for simplicity). Assuming a weak nonlinearity as well as weak (negative) damping, we can make the ansatz

$$X(t) = A(t)\cos\omega_0 t, \tag{25}$$

where $A(t)$ is a slowly varying function of time. Inserting this ansatz into the equation of motion (24) and using the fact that $A(t)$ varies slowly in time, we find the differential equation

$$\dot{A} - \delta A + \frac{3\alpha}{4\omega_0^2} A = 0 \tag{26}$$

for $A(t)$. In the stationary limit, $\dot{A} = 0$, we find the solutions $A = 0$ and

$$A = \left(\frac{4\delta\omega_0}{3\alpha}\right)^{1/2}. \tag{27}$$

A linear stability analysis readily shows that the solution with $A = 0$ is unstable, while the solution (27) is stable.

We close by providing an estimate of the oscillation amplitude. In principle, there are two contributions to the nonlinearity parameter α, the intrinsic nonlinearities of the cantilever as well as the nonlinearity of the tip-substrate interaction. It is natural to assume that the latter contribution dominates. On dimensional grounds, we estimate it to be of order

$$\alpha \sim \frac{\text{typical force}}{\text{mass} \cdot (\text{typical length})^3} \sim 10^{24}\text{N/kg}\,\text{m}^3. \tag{28}$$

Here, we used 100pN for the typical force, a value that follows from integrating the experimentally obtained force gradient, the cantilever mass $M \sim 0.1$mg, as well as the typical length scale of 1nm. If we assume that the negative damping is of the same order as the positive intrinsic damping of the cantilever, i.e., $\delta \sim 10\text{s}^{-1}$, and use the eigenfrequency $\omega_0 \simeq 10^5\text{s}^{-1}$, we find an oscillation amplitude of order $A \sim 1$nm. Although this is clearly a rough estimate of the oscillation amplitude, the result is consistent with the experimental observation and supports the picture of cantilever self-oscillations driven by current-induced switching.

[1] CreaTec Fischer & Co. GmbH, Magnusstr. 11, 12489 Berlin, Germany.

[2] F.J. Giessibl, Advances in atomic force microscopy, *Rev. Mod. Phys.* **75**, 949 (2003).

[3] Nanonis by SPECS Zurich GmbH, Technoparkstrasse 1 8005 Zurich, Switzerland.

[4] I. Horcas, R. Fernandez, J.M. Gomez-Rodriguez, J. Colchero, J. Gomez-Herrero, and A.M. Baro, WSXM: A software for scanning probe microscopy and a tool for nanotechnology. *Rev. Sci. Instrum.* **78**, 013705 (2007). 013705 (2007).

[5] J. Gupta, C. Lutz, A. Heinrich, D. Eigler, Strongly coverage-dependent excitations of adsorbed molecular hydrogen, *Phys. Rev. B*, **71** 115416 (2005).

[6] M. Heyde, M. Sterrer, G. Simon, H.-P. Rust, H.-J. Freund, Probing Adsorption Sites on Thin Oxide Films by Dynamic Force Microscopy, *Appl. Phys. Lett.* **89**, 263107 (2006).

[7] We define the quality factor Q from the fraction ν_0/BW, where BW is the full width of the resonance at $1/\sqrt{2}$ of its height.

[8] M. Ternes, Ch. P. Lutz, C. F. Hirjibehedin, F. J. Giessibl, and A. J. Heinrich, The Force Needed to Move an Atom on a Surface, *Science* **319**, 1066 (2008).

[9] J. E. Sader, S.P. Jarvis, Accurate formulas for interaction force and energy in frequency modulation force spectroscopy, *App. Phys. Lett.* **84**, 1801 (2004).

[10] L. Gammaitoni, P. Hänggi, P. Jung, and F. Marchesoni, Stochastic Resonance, *Rev. Mod. Phys.* **70**, 223 (1998).

References and Notes

1. R. D. Astumian, M. Bier, Mechanochemical coupling of the motion of molecular motors to ATP hydrolysis. *Biophys. J.* **70**, 637 (1996). doi:10.1016/S0006-3495(96)79605-4 Medline

2. J. K. Douglass, L. Wilkens, E. Pantazelou, F. Moss, Noise enhancement of information transfer in crayfish mechanoreceptors by stochastic resonance. *Nature* **365**, 337 (1993). doi:10.1038/365337a0 Medline

3. K. Wiesenfeld, F. Moss, Stochastic resonance and the benefits of noise: From ice ages to crayfish and SQUIDs. *Nature* **373**, 33 (1995). doi:10.1038/373033a0 Medline

4. S. I. Kiselev *et al*., Microwave oscillations of a nanomagnet driven by a spin-polarized current. *Nature* **425**, 380 (2003). doi:10.1038/nature01967 Medline

5. L. Gammaitoni, P. Hänggi, P. Jung, F. Marchesoni, Stochastic resonance. *Rev. Mod. Phys.* **70**, 223 (1998). doi:10.1103/RevModPhys.70.223

6. B. C. Stipe, M. A. Rezaei, W. Ho, Inducing and viewing the rotational motion of a single molecule. *Science* **279**, 1907 (1998). doi:10.1126/science.279.5358.1907 Medline

7. J. Gupta, C. Lutz, A. Heinrich, D. Eigler, Strongly coverage-dependent excitations of adsorbed molecular hydrogen. *Phys. Rev. B* **71**, 115416 (2005). doi:10.1103/PhysRevB.71.115416

8. W. H. Thijssen, D. Djukic, A. F. Otte, R. H. Bremmer, J. M. van Ruitenbeek, Vibrationally induced two-level systems in single-molecule junctions. *Phys. Rev. Lett.* **97**, 226806 (2006). doi:10.1103/PhysRevLett.97.226806 Medline

9. F. J. Giessibl, Atomic resolution on Si(111)-(7x7) by noncontact atomic force microscopy with a force sensor based on a quartz tuning fork. *Appl. Phys. Lett.* **76**, 1470 (2000). doi:10.1063/1.126067

10. Materials and methods are available as supporting material on *Science* online.

11. A. Halbritter, P. Makk, S. Csonka, G. Mihaly, Huge negative differential conductance in Au-H_2 molecular nanojunctions. *Phys. Rev. B* **77**, 075402 (2008). doi:10.1103/PhysRevB.77.075402

12. M. Trouwborst, E. Huisman, S. van der Molen, B. van Wees, Bistable hysteresis and resistance switching in hydrogen-gold junctions. *Phys. Rev. B* **80**, 081407 (2009). doi:10.1103/PhysRevB.80.081407

13. R. Temirov, S. Soubatch, O. Neucheva, A. C. Lassise, F. S. Tautz, A novel method achieving ultra-high geometrical resolution in scanning tunnelling microscopy. *New J. Phys.* **10**, 053012 (2008). doi:10.1088/1367-2630/10/5/053012

14. C. Weiss *et al*., Imaging Pauli repulsion in scanning tunneling microscopy. *Phys. Rev. Lett.* **105**, 086103 (2010). doi:10.1103/PhysRevLett.105.086103 Medline

15. B. C. Stipe, M. A. Rezaei, W. Ho, Single-molecule vibrational spectroscopy and microscopy. *Science* **280**, 1732 (1998). doi:10.1126/science.280.5370.1732 Medline

16. R. H. Smit *et al*., Measurement of the conductance of a hydrogen molecule. *Nature* **419**, 906 (2002). doi:10.1038/nature01103 Medline

17. F. J. Giessibl, Advances in atomic force microscopy. *Rev. Mod. Phys.* **75**, 949 (2003). doi:10.1103/RevModPhys.75.949

18. D. Djukic *et al*., Stretching dependence of the vibration modes of a single-molecule Pt-H_2-Pt bridge. *Phys. Rev. B* **71**, 161402 (2005). doi:10.1103/PhysRevB.71.161402

19. T. Brumme *et al*., Dynamical bistability of single-molecule junctions: A combined experimental and theoretical study of PTCDA on Ag(111). *Phys. Rev. B* **84**, 115449 (2011). doi:10.1103/PhysRevB.84.115449

20. T. Kudernac *et al*., Electrically driven directional motion of a four-wheeled molecule on a metal surface. *Nature* **479**, 208 (2011). doi:10.1038/nature10587 Medline

21. H. L. Tierney *et al*., Experimental demonstration of a single-molecule electric motor. *Nat. Nanotechnol.* **6**, 625 (2011). doi:10.1038/nnano.2011.142 Medline

22. G. A. Steele *et al*., Strong coupling between single-electron tunneling and nanomechanical motion. *Science* **325**, 1103 (2009). doi:10.1126/science.1176076 Medline

23. B. Lassagne, Y. Tarakanov, J. Kinaret, D. García-Sanchez, A. Bachtold, Coupling mechanics to charge transport in carbon nanotube mechanical resonators. *Science* **325**, 1107 (2009). doi:10.1126/science.1174290 Medline

24. S. P. Fletcher, F. Dumur, M. M. Pollard, B. L. Feringa, A reversible, unidirectional molecular rotary motor driven by chemical energy. *Science* **310**, 80 (2005). doi:10.1126/science.1117090 Medline

25. I. Horcas *et al*., WSXM: A software for scanning probe microscopy and a tool for nanotechnology. *Rev. Sci. Instrum.* **78**, 013705 (2007). doi:10.1063/1.2432410 Medline

26. CreaTec Fischer & Co. GmbH, Magnusstrasse 11, 12489 Berlin, Germany.

27. Nanonis by SPECS Zurich GmbH, Technoparkstrasse 1, 8005 Zurich, Switzerland.

28. M. Heyde, G. H. Simon, H.-P. Rust, H.-J. Freund, Probing adsorption sites on thin oxide films by dynamic force microscopy. *Appl. Phys. Lett.* **89**, 263107 (2006). doi:10.1063/1.2424432

29. We define the quality factor Q from the fraction ν_0/BW, where BW is the full width of the resonance at $1/\sqrt{2}$ of its height.

30. M. Ternes, C. P. Lutz, C. F. Hirjibehedin, F. J. Giessibl, A. J. Heinrich, The force needed to move an atom on a surface. *Science* **319**, 1066 (2008). doi:10.1126/science.1150288 Medline

31. J. E. Sader, S. P. Jarvis, Accurate formulas for interaction force and energy in frequency modulation force spectroscopy. *Appl. Phys. Lett.* **84**, 1801 (2004). doi:10.1063/1.1667267